Chemical Engineering Journal 168 (2011) 722–730

Contents lists available at ScienceDirect

Chemical Engineering Journal

journal homepage: www.elsevier.com/locate/cej

Adsorption of methylene blue on activated carbon produced from flamboyant pods (*Delonix regia*): Study of adsorption isotherms and kinetic models

Alexandro M.M. Vargas, André L. Cazetta, Marcos H. Kunita, Taís L. Silva, Vitor C. Almeida*

Department of Chemistry, Universidade Estadual de Maringá, Av. Colombo 5790, CEP 87020-900, Maringá, Paraná, Brazil

ARTICLE INFO

Article history:
Received 19 November 2010
Received in revised form 17 January 2011
Accepted 17 January 2011

Keywords:
Methylene blue
Activated carbon
Flamboyant pods
Adsorption

ABSTRACT

The adsorption of methylene blue (MB) onto activated carbon produced from flamboyant pods (*Delonix regia*) and obtained under optimized conditions (AC_{op}) was carried out in this work. The experimental equilibrium data were analyzed using the isotherms of Langmuir, Freundlich, Jovanovic, Harkins–Jura, Tempkin, Redlich–Peterson, Toth, Radke–Prausnitz, Sips, Vieth–Sladek, and Brouers–Sotolongo. The adsorption kinetics of pseudo-first order, pseudo-second order, and Avrami were used for the kinetic studies. For the Toth isotherm, the value of maximum adsorption capacity ($Q_m = 889.58\ mg\ g^{-1}$) was close to the experimental value ($Q_m = 890\ mg\ g^{-1}$), and the correlation coefficient (R^2) was 0.9836. The experimental data fitted very well to Avrami kinetic model. The Fourier-transform infrared spectroscopy spectra and the scanning electron microscopy images showed the presence of MB adsorbed onto AC_{op}. Several possible mechanisms of interaction that can occur in the MB–AC_{op} system are discussed. AC_{op} is a fast and effective adsorbent for removing MB from aqueous solutions.

1. Introduction

Dyes are widely used in industries such as the textile, paper, pulp mill, leather, dye synthesis, printing, food, and plastics industries. Since many of the organic dyestuffs are harmful to human beings and toxic to microorganisms, removal of dyestuffs from wastewater has received considerable attention over the past decades [1,2]. Most of these dyes pose acute problems for the ecological system, as they are toxic and have carcinogenic properties, which make the water contaminated with dyes inhibitory to aquatic life. Textile industries produce significant amounts of wastewater containing dyes. The main sources of wastewater generated by the textile industry originate from the washing and bleaching of natural fibers and from the fabric dyeing and finishing steps. Given the great variety of fibers, dyes and process aids, these processes generate wastewater of great chemical complexity and diversity [3]. Many types of dyes, such as direct, reactive, acid, and basic dyes, are used in the textile industry [3].

With industrialization, the discharge of industrial wastewater has increased. At the same time, there are environmental concerns, and there is the need to find cheap and efficient methods for the treatment of industrial wastewater prior to disposal into natural waters [4,5]. The most efficient method for the removal of dyes from aqueous effluents is the adsorption process [6]. Various adsorbents, such as activated bituminous coal [3], clay [4], neem (*Azadirachta indica*) leaf powder [2], jute fiber carbon [7], Abu-Tartour phosphate rock [8], black stone cherries [9], Jordanian diatomite [6], hazelnut shell [10], spent activated clay [1], bamboo activated carbon [11], coir pith carbon [12], Egyptian rice hull [13], vetiver root activated carbon [14], rattan sawdust [15], activated carbon from oil palm wood [16], garlic peel [17], and montmorillonite clay [18] have been studied for adsorption of methylene blue from aqueous solutions. Among the adsorbents mentioned, the activated carbons (ACs) have the highest dye removal efficiency due to their large surface area and the functional groups on their surface that facilitate interactions with various dyes.

Methylene blue (MB) is the cationic dye that is most commonly used for coloring. It is generally used for dyeing cotton, wool, and silk. MB can cause eye burns in humans and animals, methemoglobinemia, cyanosis, convulsions, tachycardia, dyspnea, irritation to the skin, and if ingested, irritation to the gastrointestinal tract, nausea, vomiting, and diarrhea [7]. This dye has been studied because of its known strong adsorption onto solids, and it often serves as a model compound for removing organic contaminants and colored bodies from aqueous solutions [11].

Previous studies described the preparation, characterization, and optimization based on response surface methodology [19,20], of microporous activated carbon produced from flamboyant pods (*Delonix regia*). The objective of this work was to study the removal of methylene blue from aqueous solutions using this activated carbon prepared under optimized conditions (AC_{op}). In order to establish the removal capacity of this adsorbent, different models of

* Corresponding author. Tel.: +55 44 3261 3678; fax: +55 44 3261 4334.
E-mail address: vcalmeida@uem.br (V.C. Almeida).

1385-8947/$ – see front matter © 2011 Elsevier B.V. All rights reserved.
doi:10.1016/j.cej.2011.01.067

Table 1
Physical and chemical properties of the adsorbent (AC_{op}).

Physical properties	
BET surface area ($m^2\,g^{-1}$)[a]	2854
Total pore volume ($cm^3\,g^{-1}$)[a]	1.60
Micropore volume ($cm^3\,g^{-1}$)[a]	1.44
Mesopore volume ($cm^3\,g^{-1}$)[a]	0.16
Percent micropores (%)[a]	90
Percent mesopores (%)[a]	10
Pore diameter (nm)[a]	2.24
Chemical properties	
pH_{drift}	2.01
Carboxylic groups ($mmol\,g^{-1}$)	0.92
Phenolic groups ($mmol\,g^{-1}$)	0.38
Acidic groups ($mmol\,g^{-1}$)	1.30
Basic groups ($mmol\,g^{-1}$)	0.87
Total ($mmol\,g^{-1}$)	2.17

[a] Values obtained in a previous study [20].

isotherms and adsorption kinetics were fitted to the experimental data. The Fourier-transform infrared spectroscopy (FT-IR) and scanning electron microscopy (SEM) analyses were used to assess the adsorbent material before and after dye adsorption. Finally, some possible mechanisms of adsorption are discussed.

2. Materials and methods

2.1. Adsorbent

The AC_{op} was prepared by chemical activation with NaOH using flamboyant pods (*D. regia*), as reported in the literature [20]. The physical and chemical properties of the adsorbent (AC_{op}) are presented in Table 1.

2.2. Adsorbate

The cationic dye, methylene blue (MB) or Basic Blue 9 (B. Herzog, Germany), was used as an adsorbate in this work. It has the molecular formula $C_{16}H_{18}N_3SCl$ and the molecular weight of 319.85 g mol^{-1}. The chemical structure of MB is shown in Fig. 1.

2.3. Batch adsorption studies

A stock solution of 1.0 g L^{-1} was prepared by dissolving the appropriate amount of MB in 100 mL and completing to 1000 mL with distilled water. Batch adsorption was performed in a set of 50-mL plastic flasks containing 25 mL of MB solutions with various initial concentrations (100–1000 mg L^{-1}). The amount of 0.025 g of AC_{op} was added to each flask and kept at 25 °C on a shaker. For equilibrium studies, the experiment was carried out for 2.5 h to ensure equilibrium was reached. Previous tests were performed varying the solution pH from 2 to 10 and the MB removal of approximately 90% in all pH range was determined. Therefore, the pH 6.5 was selected because favors the adsorption system MB–AC_{op}. All samples were filtered prior to analysis (using 0.45-μm membrane filters) in order to minimize interference of small particles of the activated carbon. The concentrations of MB in the supernatant solutions before and after adsorption were determined using a UV–Vis spectrophotometer (Varian Cary 50 UV/Vis) at its maximum wavelength (λ) of 664 nm. The MB concentration was determined by comparing absorbance to a calibration curve previously obtained. All experiments were duplicated and only the mean values were reported. The amount of MB adsorbed onto AC_{op}, q_e (mg g^{-1}) was calculated by Eq. (1):

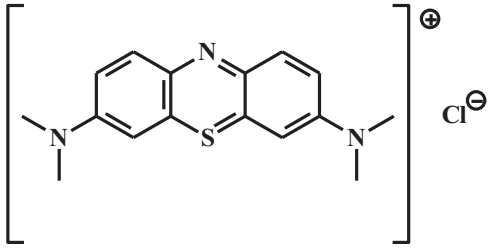

Fig. 1. Structure of methylene blue dye.

$$q_e = \frac{(C_0 - C_e)V}{W} \quad (1)$$

where C_0 and C_e (mg L^{-1}) are the initial and equilibrium liquid-phase concentrations of MB, respectively, V (L) is the volume of the solution, and W (g) is the mass of dry adsorbent used. For batch kinetic studies, the same procedure was followed, but the aqueous samples were taken at preset time intervals. The concentrations of MB were similarly measured. The amount of MB adsorbed at any time, q_t (mg g^{-1}), was calculated by Eq. (2):

$$q_t = \frac{(C_0 - C_t)V}{W} \quad (2)$$

where C_t (mg L^{-1}) is the liquid-phase concentration of MB at any time. Initial concentrations of 800, 900, and 1000 mg L^{-1} of the dye and an adsorption time of 150 min (30-min intervals) were studied. The normalized standard deviation, Δq_e (%), was calculated by Eq. (3):

$$\Delta q_e \ (\%) = 100\sqrt{\frac{\sum[(q_{e,exp} - q_{e,cal})/q_{e,exp}]^2}{N-1}} \quad (3)$$

where N is the number of data points, $q_{e,exp}$ and $q_{e,cal}$ (mg g^{-1}) are the experimental and calculated equilibrium adsorption capacity value, respectively.

2.4. Adsorption isotherm and kinetic models

The application of adsorption isotherms is very useful to describe the interaction between the adsorbate and the adsorbent of any system. The parameters obtained from the different models provide important information on the sorption mechanisms and the surface properties and affinities of the adsorbent. There are several equations for analyzing experimental adsorption equilibrium data, being that the most accepted surface adsorption models for single solute systems are the Langmuir and Freundlich model. However, an interesting trend in the isotherm modeling is the derivation in more than one approach, thus directing to the difference in the physical interpretation of the model parameters. Therefore, in this study, the isotherms of two parameters (Langmuir [3,8,11,12], Freundlich [3,8,11,12], Harkins–Jura [21], Jovanovic [21] and Tempkin [12,21,22]) and three parameters (Sips [22–25], Vieth–Sladek [24,25], Redlich–Peterson [3,14,22], Radke–Prausnitz [23–25], Brouers–Sotolongo [14], and Toth [22–25]) were applied. Table 2 shows the equations and parameters of such isotherms. The theoretical model most appropriately that describes the experimental data of the MB–AC_{op} system was chosen from the adsorption capacity (Q_m), correlation coefficient (R^2) values, and normalized standard deviation (Δq_e).

On the other hand, to understand the dynamics of adsorption in relation to time in the MB–AC_{op} system, pseudo-first order [4,6,8,10,26], pseudo-second order [4,6,8,10,26], and Avrami [27,28] kinetic models were used. Table 3 shows the equations and parameters of these kinetic models. All models were fit employing the non-linear fitting method by Origin 6.0 software.

Table 2
The names and non-linear forms of studied two-parameter (Langmuir, Freundlich, Jovanovic, Harkins–Jura, Tempkin) and three-parameter (Redlich–Peterson, Toth, Radke–Prausnitz, Sips, Vieth–Sladek, Brouers–Sotolongo) isotherm models.

Langmuir	$q_e = \frac{Q_m K_a C_e}{1+K_a C_e}$	Redlich–Peterson	$q_e = \frac{A_{RP} C_e}{1+B_{RP} C_e^g}$
	$R_L = \frac{1}{1+K_a C_0}$	Toth	$q_e = Q_m C_e (b_{To} + C_e^{n_{To}})^{-1/n_{To}}$
Freundlich	$q_e = K_F C_e^{1/n_F}$	Radke–Prausnitz	$q_e = \frac{K_{RP} Q_m C_e}{(1+K_{RP} C_e)^{m_{RP}}}$
Jovanovic	$q_e = Q_m(1 - e^{(K_J C_e)})$	Sips	$q_e = \frac{Q_m (K_S C_e)^{m_S}}{1+(K_S C_e)^{m_S}}$
Harkins–Jura	$q_e = \left(\frac{A_{HJ}}{B_{HJ} - \log C_e}\right)^{1/2}$	Vieth–Sladek	$q_e = K_{VS} C_e + \frac{Q_m \beta_{VS} C_e}{1+\beta_{VS} C_e}$
Tempkin	$q_e = \frac{RT}{b_T} \ln(k_T C_e)$	Brouers–Sotolongo	$q_e = Q_m(1 - \exp(-K_{BS}(C_e)^\alpha))$

Q_m = maximum adsorption capacity; K_a = Langmuir constant; R_L = separation factor; K_F, n_F = Freundlich constants; K_J = Jovanovic constant; A_{HJ}, B_{HJ} = Harkins–Jura constants; b_T, k_T = Tempkin constants; R = universal gas constant; T = absolute solution temperature in Kelvin; A_{RP}, B_{RP}, g = Redlich–Peterson constants; b_{To}, n_{To} = Toth constants; K_{RP}, m_{RP} = Radke–Prausnitz constants; K_S, m_S = Sips constants; K_{VS}, β_{VS} = Vieth–Sladek constants; K_{BS}, α = Brouers–Sotolongo constants.

Table 3
The names and non-linear forms of studied kinetic models.

Pseudo-first order	$q_t = q_e[1 - \exp(-k_1 t)]$ $h_0 = k_1 q_e$
Pseudo-second order	$q_t \frac{k_2 q_e^2 t}{1+k_2 q_e t}$ $h_0 = k_2 q_e^2$
Avrami	$q_t = q_e\{1 - \exp[-(k_{AV} t)]^{n_{AV}}\}$

k_1 = rate constant for the pseudo-first order adsorption; k_2 = rate constant for the pseudo-second order adsorption; h_0 = initial adsorption rate; k_{AV}, n_{AV} = Avrami constants.

2.5. Fourier-transform infrared spectroscopy (FT-IR), scanning electron microscopy (SEM), pH drift method, and Boehm titration

The surface organic structures of the AC_{op}, MB, and MB adsorbed onto AC_{op} were studied by FT-IR spectra recorded at 4 cm^{-1} of resolution and 20 scans min^{-1} between 4000 and 400 cm^{-1} using a Bomem MB-100 Spectrometer. Test discs were prepared by mixing 1 mg of sample with 500 mg of KBr (Merck for spectroscopy) in an agate mortar and then pressing the resulting mixture at 5 tons cm^{-2} for 5 min. The morphology of the AC_{op} and methylene blue adsorbed onto AC_{op} was examined by SEM (Shimadzu, model SS 550). The surface of the AC_{op} was chemically characterized by Boehm titration [29] and pH drift method [30].

3. Results and discussion

3.1. Isotherm data analysis

The values of the maximum adsorption amount (Q_m), correlation coefficient (R^2), and the other parameters for all the isotherms are shown in Table 4. The Langmuir isotherm assumes that adsorption occurs on a homogeneous surface containing sites with equal energy and that are equally available for adsorption. This is valid for the complete monolayer of adsorption, on which there is no transmigration of adsorbate on the surface plane. The Q_m value of 874.68 mg g^{-1} obtained for this isotherm is close to the experimental value of Q_m (890 mg g^{-1}), and the value of R^2 of 0.9835 shows good fitting of this isotherm to the experimental data (Fig. 2a). The separation factor (R_L), an important parameter of the Langmuir isotherm, can be used to verify if the adsorption in the system studied is unfavorable ($R_L > 1$), linear ($R_L = 1$), favorable ($0 < R_L < 1$), or irreversible ($R_L = 0$). In the concentration range studied (100–1000 mg L^{-1}), the values between 1.22×10^{-3} and 1.22×10^{-4} indicate favorable adsorption in the MB–AC_{op} system. The decrease in R_L with an increase in the initial concentration indicates that the adsorption is more favorable at high concentrations (Fig. 2b).

The Freundlich isotherm is an empirical equation that can be used for heterogeneous systems with interaction between the molecules adsorbed. The n_F parameter, known as the heterogeneity factor, can be used to indicate whether the adsorption is linear ($n_F = 1$), whether it is a chemical process ($n_F < 1$), or whether a physical process is favorable ($n_F > 1$). On the other hand, the values of $1/n_F < 1$ and $1/n_F > 1$ indicate a normal Langmuir isotherm and cooperative adsorption, respectively. The values of $n_F = 43.09$ and $1/n_F = 0.023$ indicate that the physical process and the normal Langmuir isotherm are favorable. The fitting of the Freundlich isotherm to the experimental data ($R^2 = 0.9828$) is shown in Fig. 2a. Like the Freundlich isotherm, the Tempkin isotherm considers the interactions between adsorbates assuming that the adsorption heat of all molecules decreases linearly when the layer is covered and that the adsorption has a maximum energy distribution of uniform bond. The constant b_T is related to the heat of adsorption, and the positive value found ($b_T = 107.64$) indicates an exothermic process. The fit to experimental data ($R^2 = 0.9144$) in Fig. 3a shows that the Tempkin isotherm is less adequate to explain the adsorp-

Table 4
Langmuir, Freundlich, Harkins–Jura, Jovanovic, Tempkin, Sips, Toth, Vieth–Sladek, Redlich–Peterson, Radke–Prausnitz, and Brouers–Sotolongo model constants and correlation coefficients for the adsorption of MB onto activated carbon (AC_{op}).

Langmuir	Freundlich	Harkins–Jura	Jovanovic	Tempkin
Two-parameter isotherm models				
$Q_m = 874.68$	$K_F = 791.80$	$A_{HJ} = 31.15 \times 10^3$	$Q_m = 872.86$	$b_T = 107.64$
$K_a = 8.21$	$n_F = 43.09$	$B_{HJ} = 19.67$	$K_J = -1.9351$	$k_T = 1.01 \times 10^{15}$
$R^2 = 0.9835$	$R^2 = 0.9828$	$R^2 = 0.9496$	$R^2 = 0.9836$	$R^2 = 0.9144$
Δq_e (%) = 2.85	Δq_e (%) = 1.28	Δq_e (%) = 1.22	Δq_e (%) = 4.85	Δq_e (%) = 1.30

Sips	Toth	Vieth–Sladek	Redlich–Peterson	Radke–Prausnitz	Brouers–Sotolongo
Three-parameter isotherm models					
$Q_m = 877.96$	$Q_m = 889.58$	$Q_m = 825.60$	$A_{RP} = 27.29 \times 10^3$	$Q_m = 848.72$	$Q_m = 872.86$
$K_S = 1.62$	$n_{To} = 0.45$	$K_{VS} = 0.62$	$B_{RP} = 33.68$	$K_{RP} = 8.59$	$K_{BS} = 1.37$
$M_S = 3.20$	$b_{To} = 0.06$	$\beta_{VS} = 22.63$	$g = 0.98$	$M_{RP} = 0.99$	$\alpha = 2.43$
$R^2 = 0.9836$	$R^2 = 0.9836$	$R^2 = 0.9825$	$R^2 = 0.9830$	$R^2 = 0.9835$	$R^2 = 0.9836$
Δq_e (%) = 5.20	Δq_e (%) = 2.11	Δq_e (%) = 2.08	Δq_e (%) = 1.57	Δq_e (%) = 2.17	Δq_e (%) = 6.73

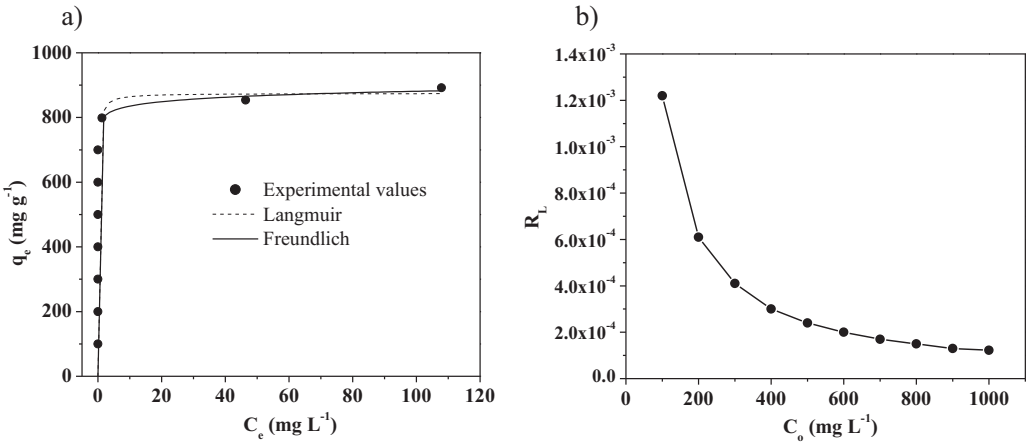

Fig. 2. Fits of the Langmuir and Freundlich isotherms (a), and Langmuir separation factor (b).

tion of MB onto AC_{op}, as compared to the Langmuir and Freundlich isotherms.

The Harkins–Jura isotherm considers the multilayer adsorption, and it can be explained by the existence of a heterogeneous pore distribution. This isotherm (Fig. 3a) showed a low correlation coefficient ($R^2 = 0.9496$), just like the Tempkin isotherm. The Jovanovic isotherm describes a model that is very similar to the Langmuir, considering a monolayer and no lateral interactions. The values of Q_m (872.86 and 874.68 mg g^{-1} for the Jovanovic and Langmuir isotherms, respectively) and R^2 (0.9836 and 0.9835 for the Jovanovic and Langmuir isotherms, respectively) show the theoretical similarities between these isotherms (Fig. 3a).

The Redlich–Peterson isotherm was developed to improve the fitting between the Langmuir and the Freundlich equations. The value of parameter g shows whether the Langmuir isotherm ($g = 1$) or the Freundlich isotherm ($g = 0$) is preferable for the system. The value of 0.98 (close to 1) found for g indicates that the Langmuir isotherm is more appropriate. The Sips isotherm is a combination of the Langmuir and Freundlich isotherms. At low adsorbate concentrations, the Sips equation is reduced to the Freundlich equation. At high adsorbate concentrations, the equation provides for the adsorption capacity in the monolayer that is typical of the Langmuir isotherm. The value of $Q_m = 877.96$ mg g^{-1} found for the Sips isotherm is slightly higher than the values of Q_m

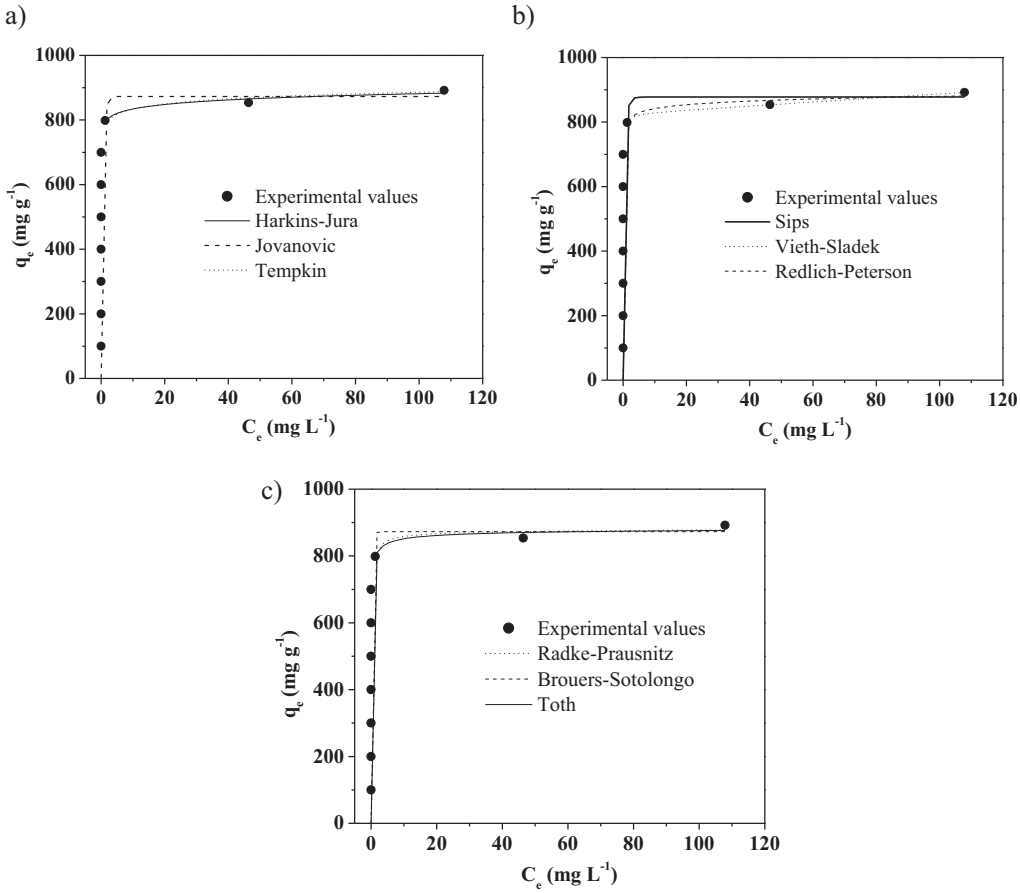

Fig. 3. Fits of the Harkins–Jura, Jovanovic, and Tempkin isotherms (a), Sips, Vieth–Sladek, and Redlich–Peterson isotherms (b), and Radke–Prausnitz, Brouers–Sotolongo, and Toth isotherms (c).

Table 5
Comparison of maximum adsorption capacity (Q_m) for MB with others adsorbents.

Adsorbent	Q_m (mg g^{-1})	Reference
Activated carbon from bituminous coal	580[a]	[3]
Clay	58.20[a]	[4]
Neem (*Azadirachta indica*) leaf powder	30.66[a]	[2]
Jute fiber carbon	225.64[b]	[7]
Abu-Tartour phosphate rock	101.13[b]	[8]
Black stones cherries	321.75[b]	[9]
Jordanian diatomite	143.3[a]	[6]
Bamboo-based activated carbon	454.20[b]	[11]
Coir pith carbon	5.87[b]	[12]
Activated carbon from Egyptian rice hull	60.10[a]	[13]
Vetiver roots activated carbon	423[b]	[14]
Garlic peel	142.86[b]	[17]
Rattan sawdust	294.12[b]	[15]
Activated carbon from oil palm wood	90.9[b]	[16]
Montmorillonite clay	300.3[b]	[18]
AC_{op} from flamboyant pods	874.68[a]–890[b]	This work

[a] Experimental.
[b] Langmuir.

for the Langmuir and Jovanovic isotherms. On the other hand, the Vieth–Sladek isotherm showed a Q_m equal to 825.60 mg g^{-1}, which was the lowest value among the isotherms that allow calculating this parameter. The fit of the Sips isotherm (R^2 = 0.9836), the Vieth–Sladek isotherm (R^2 = 0.9825), and the Redlich–Peterson isotherm (R^2 = 0.9830) to the experimental data is shown in Fig. 3b.

The Toth isotherm is another empirical equation developed to improve the fit of the Langmuir isotherm and to describe heterogeneous adsorption systems. Among all the isotherms studied, the value of Q_m equal to 889.58 mg g^{-1} found in the fit of the Toth isotherm was the value closest to the experimental one of 890 mg g^{-1}. This shows that the isotherm can be satisfactorily used in the MB–AC_{op} system. The Brouers–Sotolongo isotherm shows a Q_m value (872.86 mg g^{-1}) that is equal to that of the Jovanovic isotherm and close to the Langmuir isotherm value. On the other hand, the Q_m value equal to 848.72 mg g^{-1} found for the Radke–Prausnitz isotherm is lower than that found by the Toth and Brouers–Sotolongo isotherms. The fits of the Radke–Prausnitz (R^2 = 0.9835), Brouers–Sotolongo (R^2 = 0.9836), and the Toth (R^2 = 0.9836) isotherms to the experimental data are shown in Fig. 3c.

From the analysis of all the isotherms and the knowledge of the most important parameters (Q_m and R^2), the isotherms can be arranged according to their capacity to predict or their efficiency in predicting the experimental behavior of the MB–AC_{op} system. With respect to Q_m (in descending order): Toth > Sips > Langmuir > Jovanovic, Brouers–Sotolongo > Radke–Prausnitz > Vieth–Sladek. With respect to R^2 (in descending order): Sips, Jovanovic, Brouers–Sotolongo, Toth > Langmuir, Radke–Prausnitz > Redlich–Peterson > Freundlich > Vieth–Sladek > Harkins–Jura > Tempkin.

The normalized standard deviations (Δq_e) measures the differences in the amount of dye taken up by the adsorbent predicted by the models and the measured experimentally. According to Table 4, the Δq_e values of isotherm models ranged from 1.22 to 6.73. The Harkins–Jura and Tempkin models presented the lower Δq_e, such as the lower R^2 values. Therefore, considering the high R^2 values and Δq_e value can be observed that the Toth model is the most appropriated for the adsorption of the MB onto AC_{op}.

Table 5 shows the maximum adsorption capacity (Q_m) for various adsorbents found in the literature. Several authors present this value in the experimental form or as the maximum adsorption capacity of the monolayer obtained from the Langmuir isotherm. All the values of Q_m for the adsorption of MB are lower than the AC_{op} value obtained for flamboyant pods. The high value of Q_m obtained in this work is due to the microporous characteristic of AC_{op}, which has a BET surface area of 2854 m^2 g^{-1} (Table 1).

In previous study [19], the ACs obtained from flamboyant pods presented the highest BET surface area value in comparison to other ACs. According to the textural characterization of the AC_{op} (Table 1), the pore size distribution obtained by the HK method showed that the majority of the pores have a diameter of 2.24 nm. Considering that the width of MB molecule described by Pelekani and Snoeyink [31] is 1.43 nm, the ratio of average diameter of the AC_{op} (2.24 nm) to the width of the MB molecule could be calculated and the value of 1.57 was found. Though, the average pore diameter of AC_{op} can accommodate only one MB molecule, it has elevated porosity due the high surface area value. Therefore, the diffusion of MB from adsorbate solution to the pores of adsorbent may have been favored, which justifies the high Q_m values.

3.2. Kinetic data analysis

The kinetic adsorption data can be processed to understand the dynamics of the adsorption reactions in terms of the order of the rate constant. Since the kinetics parameters provide important information for designing and modeling the adsorption process. It is important to point out that the initial MB concentrations employed during the kinetic studies (800, 900, and 1000 mg L^{-1}) are very high when compared with other studies reported. AC_{op} has a huge adsorption capacity and adsorbs all MB when its initial concentration are lower that 800 mg L^{-1}. The kinetic data were analyzed using three different kinetic models: pseudo-first order, pseudo-second order, and Avrami equation.

The pseudo-first order model [4] is the earliest known equation describing the adsorption rate based on the adsorption capacity. The pseudo-second order model [6,8] describe that adsorption process is controlled by chemisorption which involve valency forces through sharing or exchange of electron between the solvent and the sorbate. The Avrami kinetic equation determines some kinetic parameters, as possible changes of the adsorption rates in function of the initial concentration and the adsorption time, as well as the determination of fractionary kinetic orders [28]. The conformity between the experimental data and the model-predicted values was expressed by correlation coefficients (R^2). Besides the R^2 values, the applicability of kinetics models was verified through the normalized standard deviation (Δq_e, %).

All kinetic parameters were calculated from fits of the three models (Fig. 4a–c), and they are showed in Table 6. According to Fig. 4 the models represent initial stages where a rapid adsorption occurs. The correlation coefficients for the three kinetic models (Table 6) were greater than 0.9872, which led to believe that the kinetic models provided good correlation for the adsorption to different concentrations of MB onto AC_{op}. The Δq_e values obtained for the Avrami model was 2.92%, which was the lower compared to the values of 3.05 and 7.70% obtained for the pseudo-first order and pseudo-second order kinetic models, respectively. Considering that the models presented high values of R^2, the applicability was based on the lowest Δq_e values, so the Avrami model was the most suitable equation to describe the adsorption kinetics. Moreover, the experimental q_e values agreed with the calculated values obtained from the no linear plots.

The equation of Avrami kinetic model presents Avrami exponential that is a fractionary number related with the possible changes of the adsorption mechanism that takes place during the adsorption process. So the mechanism adsorption could follow multiple kinetic orders that are changed during the contact of the adsorbate with the adsorbent [28].

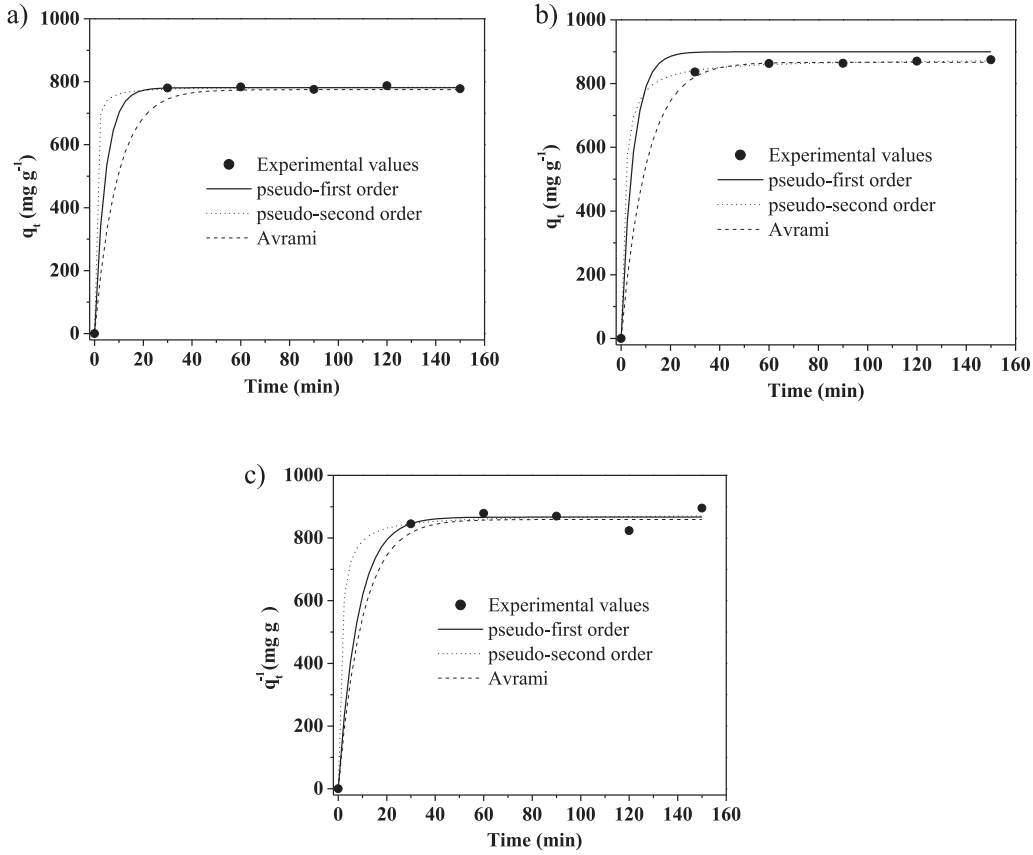

Fig. 4. Fit of pseudo-first order kinetics, pseudo-second order kinetics, and Avrami kinetics at initial concentrations of MB equal to 800 mg L^{-1} (a), 900 mg L^{-1} (b), and 1000 mg L^{-1} (c).

3.3. FT-IR spectra and SEM images of AC_{op} before and after adsorption of MB

Fig. 5 shows the FT-IR spectra for AC_{op}, MB, and MB adsorbed onto AC_{op}. In the AC_{op} spectrum (Fig. 5a), four regions (1085–1306 cm^{-1}, 1310–1448 cm^{-1}, 1450–1674 cm^{-1}, 3280–3647 cm^{-1}) stand out due to the overlapping of several bands. The bands between 1085 and 1306 cm^{-1} correspond to the angular deformation in the plane of C–H bonds of the aromatic rings (commonly appearing between 1300 and 1000 cm^{-1}), the axial deformation vibrations of the C–O bond in phenols (commonly appearing between 1260 and 1000 cm^{-1}), and the axial deformation of the C–O bond of carboxylic acid (commonly appearing between 1320 and 1210 cm^{-1}) [32]. The small band between 1310 and 1448 cm^{-1} was attributed to the interaction between the O–H angular deformation and the C–O axial deformation in phenols (commonly appearing between 1260 and 1180 cm^{-1}) and the C–O–H angular deformation of carboxylic acid (commonly appearing between 1440 and 1395 cm^{-1}) [32]. The bands between 1450 and 1674 cm^{-1} correspond to the aromatic skeletal vibrations involving the axial deformation of C–C bonds, which appear in the regions between 1600 and 1585 cm^{-1} and 1500 and 1400 cm^{-1}. According to Montes-Morán et al. [33], the bands observed in the region between 1700 and 1500 cm^{-1} were attributed to C=C symmetrical stretching of pyrone groups and C=O of carboxylic groups. The bands between 3280 and 3647 cm^{-1} correspond to the stretching of the O–H bond of free phenols or those that do not participate in hydrogen bonds (commonly appearing between 3700 and 3584 cm^{-1}), phenols with intermolecular hydrogen bonds (commonly appearing between 3550 and 3200 cm^{-1}), and O–H bond vibrations of carboxylic acid (commonly appearing between 3400 and 2400 cm^{-1}) [34].

Table 6
Kinetics parameters for the adsorption of MB onto activated carbon (AC_{op}).

C_0 (mg L^{-1})	$q_{e,exp}$ (mg g^{-1})	Pseudo-first order	Pseudo-second order	Avrami
800	778	q_e = 780.99	q_e = 710.65	q_e = 774.88
		k_1 = 0.23	k_2 = 0.005	K_{AV} = 0.33
		h_0 = 179.63	h_0 = 2525.12	n_{AV} = 0.33
		R^2 = 0.9998	R^2 = 0.9998	R^2 = 0.997
900	875	q_e = 899.58	q_e = 818.01	q_e = 866.89
		k_1 = 0.21	k_2 = 0.001	K_{AV} = 0.31
		h_0 = 188.91	h_0 = 669.14	n_{AV} = 0.31
		R^2 = 0.9872	R^2 = 0.9999	R^2 = 0.9995
1000	895	q_e = 866.70	q_e = 904.37	q_e = 859.13
		k_1 = 0.1239	k_2 = 0.001	K_{AV} = 0.32
		h_0 = 107.38	h_0 = 817.88	n_{AV} = 0.32
		R^2 = 0.9954	R^2 = 0.9952	R^2 = 0.9937
		Δq_e (%) = 3.05	Δq_e (%) = 7.70	Δq_e (%) = 2.92

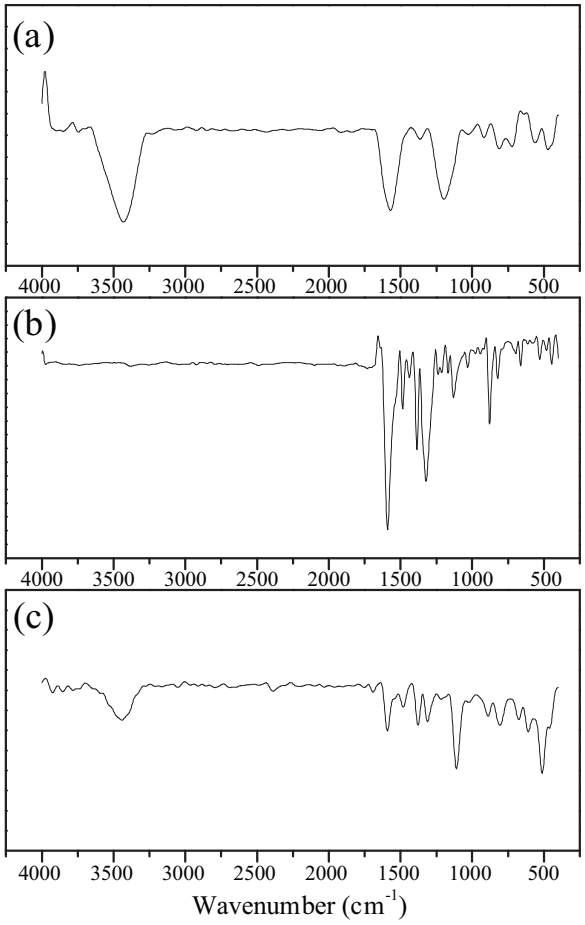

Fig. 5. FT-IR spectra of AC_{op} (a), MB (b), and MB adsorbed onto AC_{op} (c).

The spectrum of MB (Fig. 5b) shows several bands in the region between 675 and 900 cm^{-1} corresponding to axial-deformation vibrations of the C–H bond in polynuclear aromatic rings. Due to the presence of three condensed rings in the MB structure, the angular deformation bands in the C–H plane and the vibrations of C–C axial deformation for aromatic compounds, described for AC_{op}, also appear in this spectrum. The bands in the regions 1020–1250 cm^{-1} and 1266–1342 cm^{-1} were attributed to the axial deformation vibrations of the C–N bond of aliphatic amines and to the axial deformation of the C–N bond of aromatic amines, respectively [32].

The spectrum for MB adsorbed onto AC_{op} (Fig. 5c) shows new bands when compared to the spectrum of AC_{op} alone. We can clearly observe the presence of the adsorbed dye as well as some bands previously described for AC_{op} and MB. It is important to highlight that the band between 3300 and 3600 cm^{-1}, attributed to both phenolic groups and carboxylic acid, decreases in intensity because these groups interact with MB. For this reason, the band between 1550 and 1650 cm^{-1} can be attributed to the asymmetric axial deformation of the carboxylate anion, and the weaker band at 1400 cm^{-1} can be attributed to the symmetrical axial deformation of the same anion [32].

SEM analyses were performed with the purpose to confirm the adsorption of MB onto AC_{op} surface. Fig. 6a and b shows the SEM images of AC_{op} surface before and after the adsorption of MB, respectively; where the observed differences in the reflection of the images are due to the presence of MB which was adsorbed.

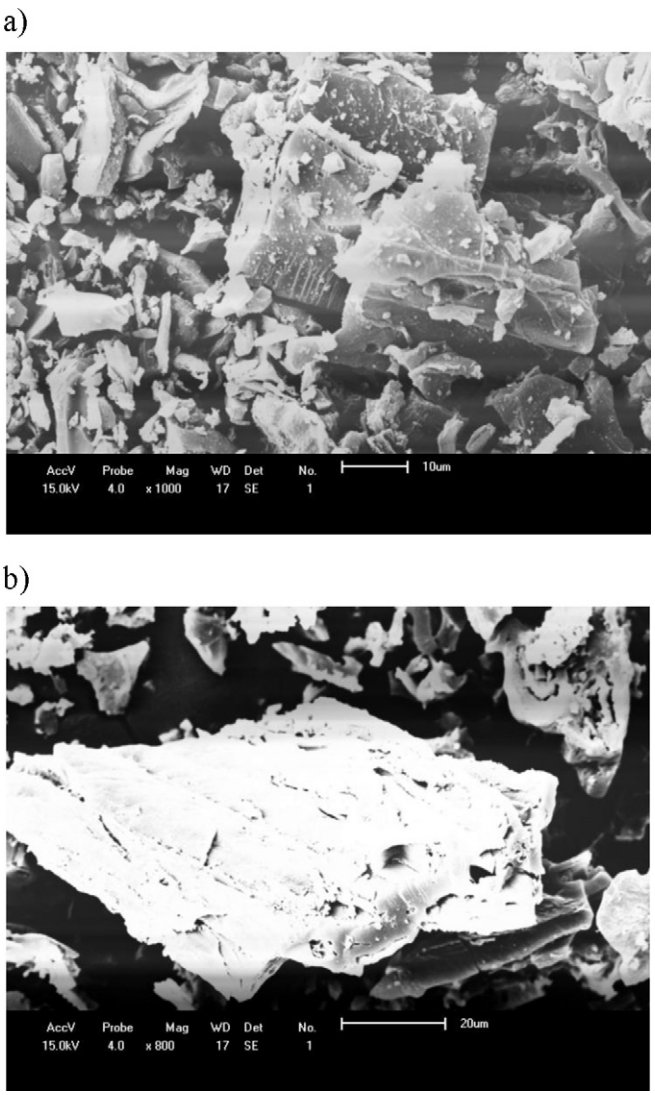

Fig. 6. Scanning electron micrographs of AC_{op} before (a) and after (b) the adsorption of MB.

3.4. Possible mechanisms of adsorption

According to Pelekani and Snoeyink [31], the width, depth, and thickness of MB are equal to 1.43, 0.61, and 0.4 nm, respectively. These dimensions allow this dye to have easy access within the porous structure of AC_{op}, which has pores that are 2.24 nm in diameter (Table 1). In addition, the adsorption process is influenced by substituent groups present in AC_{op}. The presence of surface functional groups plays an important role in the adsorption capacity and the removal mechanism of the adsorbates [13]. As demonstrated by the Boehm method (Table 1) and FT-IR analysis, the main adsorption groups to be considered for the AC_{op} are carboxylic acid, phenols, pyrones, and the aromatic structure of the graphene layer. On the other hand, due to the cationic properties of MB, its charge is delocalized throughout the chromophoric system, although it is probably more localized on the nitrogen atoms [3]. Fig. 7 shows the mechanisms that may happen in the process. The mechanisms were divided into electrostatic interactions (mechanism I), hydrogen bonding formation (mechanism II), electron donor-acceptor (mechanism III), and $\pi-\pi$ dispersion interaction (mechanism IV).

As the pH_{drift} for AC_{op} is 2.01 (Table 1), solutions with pH between 6 and 7 favor electrostatic interactions between AC_{op} and MB, because when the $pH_{solution} > pH_{drift}$, the adsorbent acquires

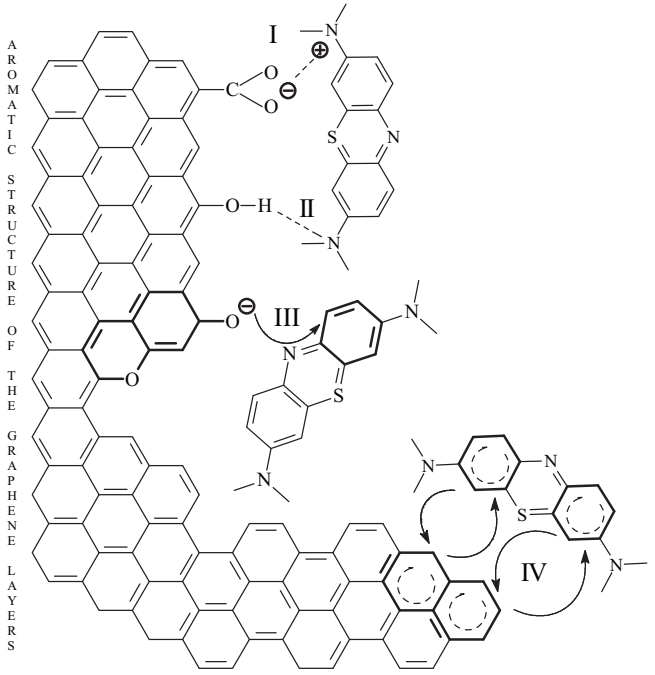

Fig. 7. Interaction mechanisms in the MB–AC_{op} system.

negative charges [30]. Furthermore, at neutral pH, there is no significant competition between the MB and the hydrogen ions for the adsorption sites.

According to mechanism I, the carboxylate anion (negatively charged) of AC_{op} can interact electrostatically with the positive charge of nitrogen present in MB. Mechanism II involves the hydrogen bonds, which are usually present in most adsorption systems and are known as non-electrostatic. Mechanism III shows that the carbonyl oxygen of pyrones present in AC_{op} can act as electron donors and the aromatic ring of MB, as an electron acceptor [35]. Pyrone groups show an increase in their basicity as more aromatic rings are added to their structure, turning them into a more polynuclear structure [33]. This creates a negative charge in the ACs, which also facilitates the interaction with positively charged adsorbates. Mechanism IV shows the π–π dispersion interaction between the aromatic ring of MB and the aromatic structure of the graphene layers [35]. Since most dyes used in the industry have aromatic rings in their structures, this mechanism should also be considered in the study of adsorption processes. Based on the Boehm method results and the BET surface area of the AC_{op}, the mechanisms mentioned earlier can present the following sequence of the importance: IV, I, III and II. The largest occurrences for the mechanism IV is due to fact that the basal plane of AC is constituted mainly of graphene layers. The mechanisms I, III and II are related with the concentration of functional groups carboxylic, pyrone and fenolic (Table 1), respectively, which are present in surface of AC_{op}.

4. Conclusions

AC_{op} proved to be an effective adsorbent for removing MB from aqueous solutions. For equilibrium studies, the isotherms were evaluated using parameters Q_m, R^2, and Δq_e. With respect to the best prediction of the Q_m value, when compared to the experimental value ($Q_m = 890\ mg\ g^{-1}$), the isotherms followed the order: Toth > Sips > Langmuir > Jovanovic, Brouers–Sotolongo > Radke–Prausnitz > Vieth–Sladek. With respect to the best fit (R^2), the order was: Sips, Jovanovic, Brouers–Sotolongo, Toth > Langmuir, Radke–Prausnitz > Redlich–Peterson > Freundlich > Vieth–Sladek > Harkins–Jura > Tempkin. Equilibrium data were best described by the Toth isotherm model with maximum adsorption capacity of $889.58\ mg\ L^{-1}$. The maximum adsorption capacity for the AC_{op} obtained on an experimental basis was higher than several adsorbents reported by the literature. The kinetic of the adsorption process was found to follow the Avrami kinetic model, which suggests the determination of fractionary kinetic orders. The functional groups present in the FT-IR spectra of AC_{op}, MB, and MB adsorbed onto AC_{op} allowed assessing the adsorption of MB, such as the SEM images. The mechanisms of electrostatic interactions, hydrogen bonding formation, electron donor–acceptor, and π–π dispersion interactions show the different interactions that may occur in the MB–AC_{op} system.

Acknowledgements

The authors acknowledge Fundação Araucária and CAPES for the financial support.

References

[1] C.-H. Weng, Y.-F. Pan, Adsorption of a cationic dye (methylene blue) onto spent activated clay, J. Hazard. Mater. 144 (2007) 355–362.
[2] K.G. Bhattacharyya, A. Sharma, Kinetics and thermodynamics of methylene blue adsorption on Neem (*Azadirachta indica*) leaf powder, Dyes Pigments 65 (2005) 51–59.
[3] E.N. El Qada, S.J. Allen, G.M. Walker, Adsorption of methylene blue onto activated carbon produced from steam activated bituminous coal: a study of equilibrium adsorption isotherm, Chem. Eng. J. 124 (2006) 103–110.
[4] A. Gürses, Ç. Doğar, M. Yalçın, M. Açıkyıldız, R. Bayrak, S. Karaca, The adsorption kinetics of the cationic dye, methylene blue, onto clay, J. Hazard. Mater. B 131 (2006) 217–228.
[5] S. Wang, Z.H. Zhu, A. Coomes, F. Haghseresht, G.Q. Lu, The physical and surface chemical characteristics of activated carbons and the adsorption of methylene blue from wastewater, J. Colloid Interface Sci. 284 (2005) 440–446.
[6] M.A. Al-Ghouti, M.A.M. Khraisheh, M.N.M. Ahmad, S. Allen, Adsorption behavior of methylene blue onto Jordanian diatomite: a kinetic study, J. Hazard. Mater. 165 (2009) 589–598.
[7] S. Senthilkumaar, P.R. Varadarajan, K. Porkodi, C.V. Subbhuraam, Adsorption of methylene blue onto jute fiber carbon: kinetics and equilibrium studies, J. Colloid Interface Sci. 284 (2005) 78–82.
[8] G.F. Malash, M.I. El-Khaiary, Methylene blue adsorption by the waste of Abu-Tartour phosphate rock, J. Colloid Interface Sci. 348 (2010) 537–545.
[9] J.M.R.R. Arana, R.R. Mazzoco, Adsorption studies of methylene blue and phenol onto black stone cherries prepared by chemical activation, J. Hazard. Mater. 180 (2010) 656–661.
[10] M. Doğan, H. Abak, M. Alkan, Adsorption of methylene blue onto hazelnut shell: kinetics, mechanism and activation parameters, J. Hazard. Mater. 164 (2009) 172–181.
[11] B.H. Hameed, A.T.M. Din, A.L. Ahmad, Adsorption of methylene blue onto bamboo-based activated carbon: kinetics and equilibrium studies, J. Hazard. Mater. 141 (2007) 819–825.
[12] D. Kavitha, C. Namasivayam, Experimental and kinetic studies on methylene blue adsorption by coir pith carbon, Bioresour. Technol. 98 (2007) 14–21.
[13] M.M. El-Halwany, Study of adsorption isotherms and kinetic models for methylene blue adsorption on activated carbon developed from Egyptian rice hull (Part II), Desalination 250 (2010) 208–213.
[14] S. Altenor, B. Carene, E. Emmanuel, J. Lambert, J.-J. Ehrhardt, S. Gaspard, Adsorption studies of methylene blue and phenol onto vetiver roots activated carbon prepared by chemical activation, J. Hazard. Mater. 165 (2009) 1029–1039.
[15] B.H. Hameed, A.L. Ahmad, K.N.A. Latiff, Adsorption of basic dye (methylene blue) onto activated carbon prepared from rattan sawdust, Dyes Pigments 75 (2007) 143–149.
[16] A.L. Ahmad, M.M. Loh, J.A. Aziz, Preparation and characterization of activated carbon from oil palm wood and its evaluation on methylene blue adsorption, Dyes Pigments 75 (2007) 263–272.
[17] B.H. Hameed, A.L. Ahmad, Batch adsorption of methylene blue from aqueous solution by garlic peel, an agricultural waste biomass, J. Hazard. Mater. 164 (2009) 870–875.
[18] C.A.P. Almeida, N.A. Debacher, A.J. Downs, L. Cottet, C.A.D. Mello, Removal of methylene blue from colored effluents by adsorption on montmorillonite clay, J. Colloid Interface Sci. 332 (2009) 46–53.
[19] A.M.M. Vargas, A.L. Cazetta, C.A. Garcia, J.C.G. Moraes, E.M. Nogami, E. Lenzi, W.F. Costa, V.C. Almeida, Preparation and characterization of activated carbon from a new raw lignocellulosic material: flamboyant (*Delonix regia*) pods, J. Environ. Manage. 92 (2011) 178–184.
[20] A.M.M. Vargas, C.A. Garcia, E.M. Reis, E. Lenzi, W.F. Costa, V.C. Almeida, NaOH-activated carbon from flamboyant (*Delonix regia*) pods: optimization of

preparation conditions using central composite rotatable design, Chem. Eng. J. 162 (2010) 43–50.
[21] M. Hadi, M.R. Samarghandi, G. McKay, Equilibrium two-parameter isotherms of acid dyes sorption by activated carbons: study of residual errors, Chem. Eng. J. 160 (2010) 408–416.
[22] P.S. Kumar, S. Ramalingam, C. Senthamarai, M. Niranjanaa, P. Vijayalakshmi, S. Sivanesan, Adsorption of dye from aqueous solution by cashew nut shell: studies on equilibrium isotherm, kinetics and thermodynamics of interactions, Desalination 261 (2010) 52–60.
[23] K.Y Foo, B.H. Hameed, Review—Insights into the modeling of adsorption isotherm systems, Chem. Eng. J. 156 (2010) 2–10.
[24] J.C. Moreno-Piraján, L. Giraldo, Adsorption of copper from aqueous solution by activated carbons obtained by pyrolysis of cassava peel, J. Anal. Appl. Pyrolysis 87 (2010) 188–193.
[25] K.V. Kumar, K. Porkodi, Relation between some two- and three-parameter isotherm models for the sorption of methylene blue onto lemon peel, J. Hazard. Mater. 138 (2006) 633–635.
[26] M.I. El-Khaiary, Kinetics and mechanism of adsorption of methylene blue from aqueous solution by nitric-acid treated water-hyacinth, J. Hazard. Mater. 147 (2007) 28–36.
[27] A.R. Cestari, E.F.S. Vieira, G.S. Vieira, L.E. Almeida, The removal of anionic dyes from aqueous solutions in the presence of anionic surfactant using aminopropylsilica—a kinetic study, J. Hazard. Mater. B 138 (2006) 133–141.
[28] E.C.N. Lopes, F.S.C. dos Anjos, E.F.S. Vieira, A.R. Cestari, An alternative Avrami equation to evaluate kinetic parameters of the interaction of Hg(II) with thin chitosan membranes, J. Colloid Interface Sci. 263 (2003) 542–547.
[29] H.P. Boehm, Some aspects of the surface chemistry of carbon blacks and other carbons, Carbon 32 (1994) 759–769.
[30] D. Prahas, Y. Kartika, N. Indraswati, S. Ismadji, Activated carbon from jackfruit peel waste by H_3PO_4 chemical activation: pore structure and surface chemistry characterization, Chem. Eng. J. 140 (2008) 32–42.
[31] C. Pelekani, V.L. Snoeyink, Competitive adsorption between atrazine and methylene blue on activated carbon: the importance of pore size distribution, Carbon 38 (2000) 1423–1436.
[32] R.M. Silverstein, F.X. Webster, D.J. Kiemle, Spectrometric Identification of Organic Compounds, 7th ed., John Wiley & Sons, New York, 2005.
[33] M.A. Montes-Morán, D. Suárez, J.A. Menéndez, E. Fuente, On the nature of basic sites on carbon surfaces: an overview, Carbon 42 (2004) 1219–1225.
[34] D.L. Pavia, G.M. Lampman, G.S. Kriz, J.R. Vyvyan, Introduction to Spectroscopy, 4th ed., Brooks/Cole, Belmont, 2009.
[35] C. Moreno-Castilla, Adsorption of organic molecules from aqueous solutions on carbon materials, Carbon 42 (2004) 83–94.